Quantum fluctuations and soliton generation in stimulated Raman scattering
by David Clyde MacPherson

A thesis submitted in partial fulfillment of the requirements for the degree of Doctor of Philosophy in Physics
Montana State University

Abstract:
Theoretical and experimental details of initiating and amplifying a Stokes pulse using stimulated Raman scattering in H2 are presented. Statistics associated with the spectral fluctuations of a Stokes seed pulse have been measured and theoretically calculated. The spectral fluctuations are shown to result from quantum noise associated with spontaneous initiation. These spectral fluctuations are an example of an easily measurable macroscopic fluctuation of quantum origin. The effects of frequency fluctuations on the generation of solitons in the nonlinear regime of stimulated Raman scattering are calculated and measured.

A detailed derivation of the fully quantum mechanical stimulated Raman scattering equations is given along with their solution for various approximations. The driven Maxwell's equation for the Raman system is derived from the system Hamiltonian. For treating the quantum initiation of stimulated Raman scattering, the radiation field is expanded in localized coherent modes. The details of calculating and using these modes to generate an ensemble of Stokes pulses are presented along with specific examples and ensemble average statistics. The use of localized modes for treating the pulsed cavityless Raman laser gives insight into the spontaneous initiation of Stokes pulses.

A numerical treatment of soliton initiation and formation in stimulated Raman scattering using a π phase shift is given. The π phase shift is produced in the Stokes seed by modulating its envelope through zero. It is found that by modulating the envelope slowly compared to the coherence decay time, T2, a soliton pulse is initiated which narrows to be much shorter than T2 Our calculations also confirm the prediction that solitons initiated using an off resonance seed decay during formation.

Solitons have also been observed in the pump and Stokes pulses from a Raman generator. It was predicted that solitons would form in the generator due to random phase shifts caused by quantum initiation. We have confirmed these predictions and measured the amplitude distribution of the spontaneous solitons.

QUANTUM FLUCTUATIONS AND SOLITON GENERATION IN STIMULATED RAMAN SCATTERING

by

David Clyde MacPherson

A thesis submitted in partial fulfillment
of the requirements for the degree

of

Doctor of Philosophy

in

Physics

MONTANA STATE UNIVERSITY
Bozeman, Montana

May 1989

APPROVAL

of a thesis submitted by

David Clyde MacPherson

This thesis has been read by each member of the thesis committee and has been found to be satisfactory regarding content, English usage, format, citations, bibliographic style, and consistency, and is ready for submission to the College of Graduate Studies.

5-12-89
Date

Chairperson, Graduate Committee

Approved for the Major Department

5-12-89
Date

Head, Major Department

Approved for the College of Graduate Studies

June 9, 1989
Date

Graduate Dean

STATEMENT OF PERMISSION TO USE

In presenting this thesis in partial fulfillment of the requirements for a doctoral degree at Montana State University, I agree that the Library shall make it available to borrowers under rules of the Library. I further agree that copying of this thesis is allowable only for scholarly purposes, consistent with "fair use" as prescribed in the U.S. Copyright Law. Requests for extensive copying or reproduction of this thesis should be referred to University Microfilms International, 300 North Zeeb Road, Ann Arbor, Michigan 48106, to whom I have granted "the exclusive right to reproduce and distribute copies of the dissertation in and from microfilm and the right to reproduce and distribute by abstract in any format."

Signature David MacPherson

Date 6/22/89

ACKNOWLEDGMENTS

I feel very fortunate to have had Dr. John Carlsten for my thesis adviser. I would like to thank John for making graduate school an enjoyable part of life and for the many hours of stimulating discussions on fundamental physics. I am also greatly indebted to my wife, Susie, for filling my big lunch bag every morning and for her many hours spent typing this thesis.

The help of Rand Swanson and Phil Battle in carefully working through and pointing out errors in my math is greatly appreciated. If there are any errors left, I will blame them. It has been great fun working with Rand Swanson and Jeff Rifkin to solve the various experimental and theoretical problems that came about during this research project.

Thanks are due to several people who added to my understanding of the fundamental details of this research. Dr. Mike Raymer provided insight and understanding for the process of quantum initiation and Dr. Kai Druhl provided theoretical support for our work on soliton initiation.

Finally, I would like to thank Dr. Richard Robiscoe and Dr. Rufus Cone who carefully read this thesis. Their comments are appreciated and have made a definite improvement. This being the last day of National Secretaries Week, I would like to thank the secretaries who have always gone out of their way to be helpful.

TABLE OF CONTENTS

APPROVAL ii

STATEMENT OF PERMISSION TO USE iii

ACKNOWLEDGMENTS iv

TABLE OF CONTENTS v

LIST OF TABLES vii

LIST OF FIGURES viii

ABSTRACT xi

1. INTRODUCTION 1

The Raman Scattering System 4
Quantum Initiation of Stimulated Raman Scattering 8
Solitons in Stimulated Raman Scattering 11

2. DERIVATION AND SOLUTION OF SRS EQUATIONS 16

Derivation of the Medium Equation 20
Derivation of the Stokes Field Equation 27
Properties of the Langevin Noise Operator 35
Retarded Time Transformation 39
Linear Solution 40
The Nonlinear Stimulated Raman Scattering Equations 41
The Soliton Solution 43
Steady State Solution 46

3. THEORY OF QUANTUM INITIATION AND AMPLIFICATION 50

Quantum Initiation 50
Coherent Mode Expansion 55
Numerical Procedure for Coherent Modes Calculation 64
Numerical Propagation Through Depletion 65
Theoretical Results 71
Discussion on Propagation Through Depletion 75
C-Number Calculation 82

TABLE OF CONTENTS -- Continued

4. QUANTUM FLUCTUATION EXPERIMENT 87

Pump Laser 87
Optical Layout 91
Multi Pass Cell Alignment 95
Detectors and Interfacing 99
Data Analysis 101
Experimental Results 105

5. THEORY OF SOLITON GENERATION AND DECAY 111

Forming a Soliton with Phase Shifts 112
Theoretical Soliton Generation at 100 Atmospheres 114
Energy Flow Between Fields and Q 120
Pulse Formation and Narrowing 124
Computer Modeling Off Resonance 131
Gain Narrowing and the Phantom Linewidth 133
Stimulated Raman Scattering in a Multi Pass Cell 138

6. SOLITON GENERATION EXPERIMENT 141

Optical Layout 141
Generating Electrooptic Phase Shifts 143
Amplification in a MPC Without Phase Shifts 146
Soliton Generation and Decay 154
Spontaneous Soliton Generation 158

7. CONCLUSIONS 164

REFERENCES CITED 170

APPENDICES 175

A. SVEA Approximation 176
B. Computer Programs 180
Gbuild 181
Control 189
Fldens 190
Bfft 192
Enscor1 197
Enlsrs 199
C. AMPS Phase Shifter 208

LIST OF TABLES

Table		Page
1.	Statistical weights of coherent modes	63
2.	Widths of the distribution of central frequencies for various standard deviation cutoffs	138

LIST OF FIGURES

Figure		Page
1.	Energy level diagram for stimulated Raman scattering	6
2.	Coherent and chaotic state photon number distribution	52
3.	Number state distribution for highly excited modes	53
4.	First three temporal modes generated using coherent modes theory	62
5.	Flow chart for generating an ensemble of spectra	66
6.	Retarded time coordinate system for nonlinear integration	68
7.	Diagram of the nonlinear integration procedure	69
8.	Theoretically generated sample of a narrow single shot Stokes spectra	72
9.	Example of a theoretically generated single shot Stokes spectra with multiple spikes	73
10.	Autocorrelation calculated from coherent modes theory	75
11.	Ensemble average power spectrum calculated using 15 temporal modes	76
12.	Temporal Stokes pulse corresponding to Figure 8	77
13.	Temporal Stokes pulse corresponding to Figure 9	78
14.	Autocorrelation before pump depletion	79
15.	Autocorrelation from the sum of two gaussians	80
16.	Ensemble average power spectrum calculated using only 3 temporal modes	82
17.	Autocorrelation calculated using c-number approach	85
18.	Autocorrelation using gain narrowed noise	86
19.	Diagram of the optical components in the pump laser	88
20.	Temporal pulse shape from the pump laser at 532nm	90
21.	Optical layout for the quantum fluctuation experiment	91

LIST OF FIGURES -- Continued

Figure		Page
22.	Spatial profile of the pump laser beam after filtering	92
23.	Optical layout of the Fabry Perot and alignment system	94
24.	Alignment diagram for the mode matching lenses and the MPC mirrors	97
25.	Raw spectral data from a corss-section of the Fabry Perot rings	101
26.	Ray diagram for the Fabry Perot interferometer with a diverging input beam	102
27.	Experimental example of a narrow single shot Stokes spectrum	106
28.	Experimental example of a single shot Stokes spectrum with several narrow spikes	107
29.	Experimental ensemble average spectrum	108
30.	Experimentally measured autocorrelation function	109
31.	Experimental examples of Stokes spectra generated at 10atm	110
32.	Diagram showing the differential change in the pump and Stokes fields	113
33.	Stokes seed intensity with the AMPS	116
34.	Pump pulse that evolves with an AMPS	117
35.	Soliton formation and evolution	118
36.	Evolution of the soliton pulse width	119
37.	Soliton narrowing in the hypertransient regime	120
38.	Three characteristic regions of the soliton pulse	121
39.	Evolution of the polarization wave	123
40.	Near hyperbolic secant form of the soliton	124
41.	Soliton formation off resonance	132
42.	Fractional soliton amplitude resulting from detuning of the Stokes seed	133

LIST OF FIGURES -- Continued

Figure		Page
43.	Theoretical distribution of soliton amplitudes based on the phantom and subphantom linewidths	137
44.	Experimental apparatus used to study the soliton initiation and decay	143
45.	Pockels cell triggering diagram	145
46.	Spatial profile of the Stokes pulse from the Raman generator	147
47.	Theoretical and experimental amplification without phase shifts	149
48.	Theoretical and experimental Stokes pulse shapes	150
49.	Spectral lineshapes for the Stokes seeds	151
50.	Experimental example of a soliton induced by a phase shift	155
51.	Comparison between theoretical and experimental results of soliton formation	156
52.	Experimentally measured distribution of induced soliton amplitudes	157
53.	Theoretical distribution of spontaneously generated soliton amplitudes	159
54.	Typical spontaneous soliton in the depletion region of the output pump pulse	161
55.	Experimentally measured distribution of spontaneous soliton amplitudes	162
56.	Computer program Gbuild	181
57.	Computer program Control	189
58.	Computer program Fldens	190
59.	Computer program Bfft	192
60.	Computer program Enscor1	197
61.	Computer program Enlsrs	199

ABSTRACT

Theoretical and experimental details of initiating and amplifying a Stokes pulse using stimulated Raman scattering in H_2 are presented. Statistics associated with the spectral fluctuations of a Stokes seed pulse have been measured and theoretically calculated. The spectral fluctuations are shown to result from quantum noise associated with spontaneous initiation. These spectral fluctuations are an example of an easily measurable macroscopic fluctuation of quantum origin. The effects of frequency fluctuations on the generation of solitons in the nonlinear regime of stimulated Raman scattering are calculated and measured.

A detailed derivation of the fully quantum mechanical stimulated Raman scattering equations is given along with their solution for various approximations. The driven Maxwell's equation for the Raman system is derived from the system Hamiltonian. For treating the quantum initiation of stimulated Raman scattering, the radiation field is expanded in localized coherent modes. The details of calculating and using these modes to generate an ensemble of Stokes pulses are presented along with specific examples and ensemble average statistics. The use of localized modes for treating the pulsed cavityless Raman laser gives insight into the spontaneous initiation of Stokes pulses.

A numerical treatment of soliton initiation and formation in stimulated Raman scattering using a π phase shift is given. The π phase shift is produced in the Stokes seed by modulating its envelope through zero. It is found that by modulating the envelope slowly compared to the coherence decay time, T_2, a soliton pulse is initiated which narrows to be much shorter than T_2. Our calculations also confirm the prediction that solitons initiated using an off resonance seed decay during formation.

Solitons have also been observed in the pump and Stokes pulses from a Raman generator. It was predicted that solitons would form in the generator due to random phase shifts caused by quantum initiation. We have confirmed these predictions and measured the amplitude distribution of the spontaneous solitons.

CHAPTER 1

INTRODUCTION

The first documented observation of a solitary wave was made in 1834 by a Scottish scientist and engineer, John Scott Russel[1]. The wave was generated when a canal barge abruptly stopped. From the turbulence a solitary wave formed which propagated one or two miles along the canal before being damped out.

At present there are examples of solitary waves or solitons in several branches of physics[1]. Solitons are localized disturbances which retain their shape as they propagate. Solitons result from a balance between the competition of two effects in a nonlinear system. The above example of water waves results from a competition between dispersion and the nonlinearity which arises when the depth of the water is comparable to the amplitude of the wave. The nonlinear equation governing wave propagation in shallow water is called the Korteweg de Vries (KdV) equation. Other equations which admit soliton solutions are the Modified KdV, sine-Gordon, and Nonlinear Schrodinger (NLS) equation.

The classic example of an optical systems which admits soliton solutions is Self Induced Transparency (SIT)[2]. For this example a coherent optical pulse propagates in a medium of two level atoms. The competition which allows soliton propagation in SIT is between absorption by the medium during the leading part of the pulse and amplification of the pulse by the medium during the trailing part of the pulse. SIT obeys the sine-Gordon equation and the nonlinear equations which govern Stimulated Raman scattering (SRS) can also be transformed into the sine-Gordon equation. Another

example of optical soliton propagation in a nonlinear medium occurs in optical fibers[3]. These solitons which are described by the NLS equation result from the balance between dispersion and an amplitude dependent nonlinearity.

The soliton in SRS is the only known example of a three wave soliton. The Raman soliton exists as a localized disturbance in two optical fields and a polarization pulse in the Raman medium. Solitons are initiated in SRS by placing phase shifts in an optical field before it enters the Raman active medium. There are two things about solitons in SRS that are of particular interest. First the solitons are to some degree stable or, in other words, they do not break apart as they propagate. The second interesting feature is that as the soliton propagates it is able to drive atoms from a sparsely populated excited state into the heavily populated ground state. This effect occurs as the later half of a soliton pulse interacts with the medium.

The goal of this research was to obtain an understanding of the fundamental interactions involved with transient Raman scattering. The intention was to investigate the propagation of intense laser pulses and study the effects of phase shifts in a transient medium. Such studies are important to establish a pool of knowledge and techniques which can be of general use in the study of laser beam propagation in a variety of systems.

At the beginning of this research project the primary goal was to study the formation and propagation of solitons in SRS. The solitons had been predicted theoretically[4] and had also been observed experimentally[5]. The first observations were accidental and the origin of the solitons was not understood. Subsequent experiments to initiate Raman solitons using sudden phase shifts did not reliably generate solitons[6]. The primary goal of my research project was to demonstrate that solitons could be reproducibly generated in SRS. In addition we wanted to obtain an understanding of how a phase shift caused a soliton to form. The effects of phase shifts in coherent scattering processes has been

virtually unexplored. In the Raman system the phase shift reverses the direction of gain. An understanding of this process may lead to new experiments in other systems.

Our experiments did in fact generate Raman solitons using laser pulses with phase shifts[7]. However, the amplitude of the generated solitons was found to vary greatly for identical experimental conditions. While investigating the cause of the amplitude variations, we discovered that the spectrum of light generated using SRS also had large fluctuations from pulse to pulse[8]. We have now determined that the spectral fluctuations were due to quantum-mechanical noise. Much of this thesis deals with the calculations and measurements of spectral fluctuations. We found that an understanding of these fluctuations was necessary to understand the statistics associated with soliton generation in SRS.

Other systems which have produced macroscopic fluctuations of quantum origin are the cavityless dye laser[9] and superfluorescence[10]. These are both examples of nonoscillating optically pumped lasers. The dye laser uses a grating for one feedback mirror. As in stimulated Raman scattering, the macroscopic fluctuations in the dye laser appear as shot to shot spectral variations. The superfluorescence system consists of a pencil shaped two level medium which is initially completely inverted. Light pulses are emitted from both ends of the medium by the collective emission of all the two level atoms. Macroscopic fluctuations appear in the time delay between inverting the system and detecting the light pulses.

Quantum noise is present to varying degrees in all light. For some cases, such as a single mode laser operating well above threshold, the noise is very small compared to the average signal. On the other hand, thermal sources have noise which is as large as the average intensity. For most cases the variations in thermal light is so rapid that it cannot be resolved. Because quantum noise is always present, it is important to understand and characterize the noise for various sources. Since Raman scattering is an important

method of shifting the frequency of a laser to obtain a light source at lower frequency, the spectral fluctuations which we observed will be important for many applications. It is often the case that understanding the light source used in an experiment is an important part of understanding the experiment.

The stimulated Raman scattering system is an example of single pass cavityless laser. Understanding quantum initiation and amplification in such a laser is helpful when trying to form a conceptual picture of how a quantized field interacts with an atomic system. Because there is no cavity, the choice of modes for expanding the field is not obvious. The research that we have done explores selecting a localized set of modes which evolve during amplification.

All lasers are initiated by spontaneous emission. Spontaneous emission results from a quantum mechanical fluctuation. For this reason I will often refer to the spontaneous emission as quantum initiation.

While our experiments were being carried out, it was predicted[11] that in addition to the phase-shift induced Raman solitons, solitons resulting from quantum noise should also be observed. These solitons are a macroscopic signal resulting from quantum noise. We were able to observe these solitons and verify the theoretically predicted[12] amplitude distribution.

The Raman Scattering System

In this section the experimental system used to perform SRS is described. The medium that was used for Raman scattering was H_2 at 10 or 30 atm. The important energy levels are shown in Figure 1. Level (1) is the ground state and level (2) is an electronic excited state. Level (3) is the lowest vibrational excited state. The levels represented by the upper and lower dashed lines are virtual or dressed states. The virtual

levels are generated by the fields which oscillate at angular frequencies ω_p and ω_s. The field oscillating at ω_p is the pump laser field which for our experiments was the output from a frequency doubled Neodymium Yttrium Aluminum Garnet (Nd:YAG) laser. The wavelength of this light is 532nm which is green. The field oscillating at ω_s is the Stokes field which grows up from spontaneous Raman emission. The wavelength of the Stokes light is 680nm which is red. When an H_2 molecule is driven by an intense field at ω_p, it will oscillate at ω_p even though there are no nearby levels. This oscillation can be thought of as arising from a superposition of level (1) and the upper virtual level. The virtual level exists to the extent that the molecule oscillates at ω_p. Because the pump field is so far off resonance, it must be very intense in order to produce a significant oscillation at ω_p.

When deriving the equations governing SRS in Chapter 2, I will allow for a possible detuning of the Stokes beam from level (3). This will be important when treating the decay of Raman solitons in Chapter 5. This detuning comes about from quantum fluctuations. Except for the detuning Δ_ϵ, the energy levels in Figure 1 have been drawn to scale.

As shown in the figure there are two possible time orderings for Raman scattering. For the upper path, a molecule absorbs a pump photon and then emits a Stokes photon leaving the molecule in the vibrational state (3). The 1-3 transition is not dipole allowed making the decay of level (3) negligible for time scales which are shorter than or equal to the duration of the pump pulse. For the opposite time ordering, the molecule first emits a Stokes photon and then absorbs a pump photon to again end up in level (3). The coupling strength of the two paths depends on the detuning of the respective virtual level from level (2). The upper virtual level is detuned by Δ_p and the lower virtual level is detuned by $\Delta_p + \omega_p + \omega_s$. Because Δ_p is so large, the lower time ordering cannot be neglected. The inclusion of the lower time ordering does not significantly complicate the

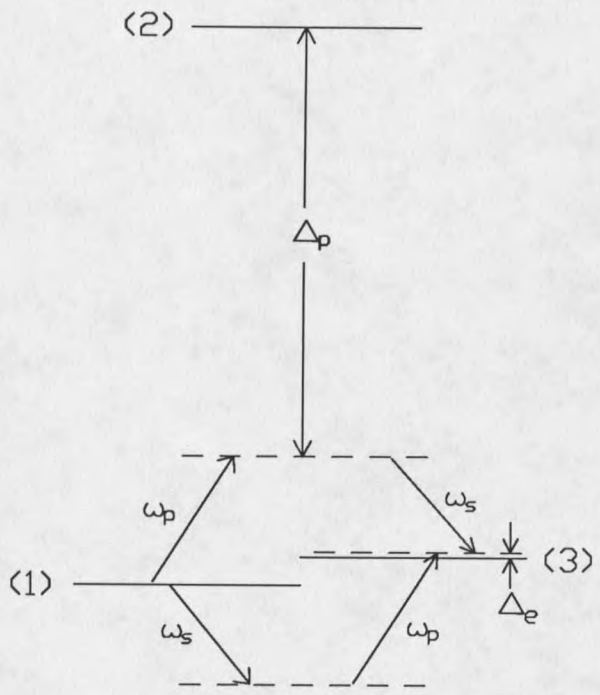

Figure 1 Energy level diagram for stimulated Raman scattering.

mathematical treatment.

There are several important time scales to consider when treating SRS. The slowest time scale is the decay of level (3) to level (1) which is on the order of milliseconds. This is such a long time that it can be considered infinite. The next slowest time scale is the duration of the pump laser pulse which is 20 to 30 nsec. The temporal shape of pulses with this duration are easily measured using a photo-diode and a 400MHz storage oscilloscope. Next on the time scale is the collisional dephasing rate (Γ) which is approximately 1/(0.6nsec) and 1/(0.18nsec) for hydrogen pressures of 10 and 30 atm respectively[13]. The fastest time scale is $1/\Delta_p$ which for our experiments is 0.037fsec.

This is the time required for a molecule to realize that the pump is not on resonance with the 1-2 transition.

The characteristic decay time associated with the collective oscillation of the medium is $1/\Gamma$. The pump and Stokes fields drive the molecules into a superposition of levels (1) and (3), and to a very small extent level (2). The amplitude in level (3) is always much less than 1. The superposition of levels (1) and (3) results in a quadrupole oscillation at $\omega_{31} = \omega_3 - \omega_1$. The phase of this oscillation is determined by the phase of the pump and Stokes field. The collective oscillation of all the atoms gives rise to a macroscopic quadrupole oscillation. When a molecule undergoes a collision, its phase is either partially or completely randomized. When a molecule's phase has been randomized, it no longer contributes to the collective oscillation.

Due to the large detuning Δ_p, the three-level system can effectively be reduced to a two-level system. The amplitude of the virtual states is always small and it comes to equilibrium very quickly allowing the turn-on effects to be neglected for the virtual states. This greatly simplifies the calculations by effectively reducing the system to a two-level problem[14]. The detuning Δ_e can then be thought of as the effective two level detuning. This detuning turns out to be very important for studying soliton generation.

The pump field generates a small amplitude in the virtual states allowing light at the Stokes frequency to be emitted by spontaneous emission. This light will be emitted in all directions and a small portion of it will be emitted in the direction of the pump laser beam. This portion of the spontaneous emission will stimulate further emission at the Stokes frequency. If the length of the medium and the intensity of the pump is large enough, the Stokes pulse will grow until portions of the pump pulse are completely depleted.

To perform SRS, the pump laser beam can simply be focussed into a long cell containing hydrogen. As will be shown, SRS is a nonlinear process requiring high

intensities so focussing is usually needed. For gaussian-like temporal pulses, the very front and back of the pump will not be depleted due to the lower intensity in those regions. For our experiments roughly 80% of the pump photons were converted into Stokes photons.

To effectively increase the length of the Raman scattering medium, we used Multi Pass Cells[15] (MPC). The MPC refocuses the pump and Stokes beams several times through the hydrogen cell. However, each focus is at a new location in the cell, so the system can be modeled as a single pass cell with many focuses. In addition to increasing the length of the medium, the MPC suppresses parasitic processes such as second Stokes scattering and anti-Stokes scattering because of dephasing in the cell windows.

Quantum Initiation of Stimulated Raman Scattering

In effect, a stimulated Raman scattering system is a single pass laser with several similarities to a laser that amplifies light which oscillates between two mirrors. Although the Raman laser does not use a population inversion in the usual sense, the Stokes pulse is initiated by spontaneous emission and is amplified to saturation similar to the initiation in a cavity laser.

In order to treat the problem of quantum initiation, the field as well as the molecules must be treated quantum mechanically[16]. For most optics problems, the semi-classical treatment, for which the medium is treated quantum mechanically and the field classically, is sufficient. In order to treat the field quantum mechanically, we must choose a set of radiation modes for describing the field. Once the modes have been chosen, quantum mechanics will tell us the probability distribution for the number of photons in each of the modes. In general, the number of photons in one mode will not be independent from the number in another mode.

In order to treat a single pass Raman laser, Raymer et al.[17] adapted a choice of modes based on the correlation function of the generated Stokes pulses. The resulting set of modes is referred to as the coherent modes. Although generating the coherent modes requires substantial numerical calculations, generating statistics using the coherent modes is simplified. The simplification results from the requirement that the level of excitation of each coherent mode is independent of the other modes. Because the modes are not correlated, ensemble members of the Stokes field can be generated by simply adding the modes together with random phases and statistically weighted amplitudes.

As a result of the quantum mechanical initiation process, macroscopic fluctuations can occur. A mode of the radiation field which grows up from spontaneous emission will be in a chaotic state until it saturates its energy sources.[18] The statistics associated with chaotic states will be given in Chapter 3. The important feature of a mode in a highly excited chaotic state is that the range of possible energies or number of photons in the mode is very broad. This is to say that an ensemble of identically prepared chaotic modes will have a significant fraction of members containing only a few photons as well as members containing large numbers of photons. This broad distribution is the source of macroscopic fluctuations in a variety of experiments. Using the coherent modes description, the statistics of Stokes pulse energies have been predicted[19]. This distribution was also measured[20] and good agreement was obtained. Our experiments involved measuring the spectral fluctuations in the Stokes pulses. Spectral fluctuations arise when more than one mode is excited into a chaotic state. A simple example of this effect is a pulsed laser which is allowed to oscillate in a few longitudinal modes. If the laser is operated below saturation each mode will be in a chaotic state. If the laser cavity has a high quality factor each mode of the laser will appear as a narrow peak in the laser spectrum. Since the energy in each mode is highly uncertain, the relative amplitudes of the peaks in the spectrum will be quite different from shot to shot[21]. This is an example

of macroscopic fluctuations which arise from the spontaneous emission.

More dramatic spectral fluctuations can be produced if the quality factor of the above described laser is decreased. This will increase the width of the spectral peaks for each cavity mode. In fact, the width can become larger than the spacing between adjacent modes. For this situation, the spectrum will have more dramatic fluctuations because the spectral peaks from various modes will interfere with each other in a random way. Since the phase of each mode is random, on some shots two adjacent modes can interfere constructively and on others destructively.

For a single pass laser, such as the Raman laser, there is no cavity to choose the modes. To treat the problem we want to use the choice of modes which makes the calculations simplest. For the coherent modes choice, the spectrum of each mode is centered at the same frequency resulting in significant overlap of many modes. This large spectral overlap give rise to large fluctuations.

We used the coherent modes theory to treat the spectral fluctuations in SRS and good agreement with experiment was obtained[22]. The details of this calculation are given in Chapter 3. Our calculations generate ensemble members of output Stokes pulses which are used to generate statistics.

In order to treat quantum fluctuations, we must know how to treat the spontaneous emission process. There are two distinct ways to interpret spontaneous emission[10,23,24]. In one interpretation, vacuum fluctuations stimulate atoms to emit a photon. This interpretation arises when anti-normal ordering of the field operators is used. The other interpretation is called radiation reaction. For this interpretation, molecular polarization fluctuations drive a radiation mode which then couples back to the molecules causing them to emit photons. The coherent modes approach uses polarization fluctuations to initiate the Stokes pulse[17]. We have also applied the vacuum field approach and obtained similar results[22].

To give an intuitive picture of how spectral fluctuations arise from the vacuum field, we need to understand the spectrum of the vacuum field. The vacuum field is considered to be white noise meaning that it has a uniform spectrum. However if one looks at the spectrum of a pulse of white noise it will not be uniform at all. The spectrum will be quite noisy with a characteristic frequency scale which is given by one over the temporal length of the pulse. The average spectrum of several pulses would give the uniform spectrum of white noise.

Our SRS experiment[8,22] with a pulsed pump laser amplifies a temporal segment of white noise. Thus when the spectrum of an individual Stokes pulse is observed, it will have fluctuations on the scale of one over the Stokes pulse length. Since SRS only amplifies a narrow range of frequencies, when the spectrum of many shots are averaged together the result will not be a uniform spectrum but rather an average spectral line shape.

Solitons in Stimulated Raman Scattering

Before describing soliton solutions I will describe what is meant by a general solution to the SRS system. The inputs to a Raman amplifier are arbitrary pump and Stokes fields. Before these pulses arrive, the molecules in the medium are assumed to be in the ground state. Given the temporal envelopes and phases of the input fields, a general solution would tell us the envelopes and phases of the fields at the exit of the Raman amplifier. Because SRS in an amplifier is described by a set of nonlinear differential equations, a general solution does not exist. The soliton solution is a special solution which is valid for a special class of input fields.

To help understand the nonlinear SRS process, it is useful to define three time scale regimes. When the envelopes of the fields vary slowly compared to the collisional

dephasing time the system is in the *steady state* regime. The opposite limit where the field envelopes vary much faster than the dephasing time is called the *hypertransient* regime. Intermediate between these situations is the *transient* regime. While our experiments probe all three regimes, the most interesting is the transient regime.

In 1975, Chu and Scott[4] considered a number of nonlinear wave-wave scattering problems using the inverse scattering transform. They found that the SRS equations admitted a soliton solution in the limit that collisional dephasing could be neglected (hypertransient regime). Damping can be neglected for pulses which are much shorter than the damping time. The form of the soliton solution is a hyperbolic secant for the pump field's temporal envelope, a hyperbolic tangent for the Stokes field envelope, and a hyperbolic secant for the oscillation in the medium as a function of time. Because there are three quantities involved, the Raman soliton is referred to as a three wave soliton. Soliton formation with more waves has also been studied[25].

We would like the solution for the fields to go to zero for times before the pulse arrives and after the pulse has passed. The $\tanh(t)$ solution for the Stokes field goes to ± 1 for $t = \pm\infty$. This boundary condition is not a significant problem as long as the Stokes pulse does not go to zero in the region of the soliton. For this case, the soliton solution is valid in the region of the soliton but does not hold in the temporal wings of the pulse.

In 1983, short pulses were observed[5] in a Raman amplifier which was pumped by a CO_2 laser. These pulses were identified as the predicted Raman solitons. Although the original theoretical calculations by Chu and Scott had not predicted how such soliton pulses could be produced, the agreement between experimental data and computer modeling by Druhl[26] using instantaneous π phase shifts in the Stokes seed indicated that the soliton like pulses were being initiated in the transient regime. Once initiated, the pulses narrowed due to damping until they were so short that damping could be neglected. Again one of the important features of the soliton pulses is that they are stable

and do not fall apart during the formation process.

The hyperbolic tangent solution for the Stokes pulse crosses through zero at the center of the soliton. This zero crossing gives a π phase shift between the front and the back of the Stokes pulse which led Druhl to use a π phase shift in the input Stokes seed for modeling the soliton formation that was originally observed. The source of the phase shifts in the original experiments were not understood. Subsequent experiments[6] in the Infra-Red (IR) in which a π phase shift was induced in the Stokes seed failed to reproducibly generate soliton pulses. The difficulties in this experiment were attributed to problems with working in the IR. It is difficult to work in the IR because most detectors including the human eyes are not sensitive in this region.

To improve on the previous experiments, we used a visible laser to pump the Raman medium. To initiate a soliton to form in a Raman amplifier, a pump laser pulse and a Stokes seed pulse were combined and injected into the amplifier cell. The Stokes seed was produced in a separate Raman generator. Before entering the amplifier, a π phase shift was produced in the seed pulse by passing it through a crystal whose index of refraction depends on the voltage applied across the crystal. The voltage on the crystal was abruptly changed when the seed pulse was half way through the crystal. This caused the latter half of the pulse to see a greater optical path length than the first half. If the change in path length is half of a wavelength, a π phase shift results between the front and back of the pulse.

As with solitons in other systems such as water waves in a narrow channel and self induced transparency[27], solitons in SRS result from the competition between two effects. The competing effects in the SRS system are forward Raman scattering before the phase shift and inverse Raman scattering after the phase shift. For inverse Raman scattering the pump pulse grows and the Stokes pulse is depleted.

The SRS equations can be transformed into the more familiar sine-Gordon equation.

The sine-Gordon equation also governs self induced transparency in which a single optical field propagates in a medium of two level atoms. Using the sine-Gordon form, Steudel[28] treated the initial pulse resulting from a π phase shift in the Stokes seed. His approximations are valid in the region before significant pump depletion occurs. Meinel[29] used the Backlund transformation to treat the problem of higher order solitons in both SRS and two-photon propagation. However no physical meaning has yet been associated with higher order solitons[30].

Considerable theoretical work has been done on the problem of treating soliton propagation when the damping is small but not small enough to be neglected. Kaup[31] developed a modified inverse scattering transform to include weak damping in the SRS soliton propagation. Druhl and Alsing[32] used a perturbative approach to include weak damping. In Chapter 5, a physical approach to the weak damping problem is presented which uses energy conservation to predict the width of the evolving soliton pulse. Numerical calculations have also been carried out for soliton generation using a Stokes seed which is off resonance[33,34]. This corresponds to a nonzero Δ_e in Figure 1. These calculations show that an off resonance seed causes the soliton pulse to decay during formation. Due to quantum fluctuations, seed pulses from the generator can be off resonance in the amplifier. Correctly predicting the statistics of soliton decay was one of the major goals of my research.

As mentioned earlier one of the properties of a soliton pulse is that it propagates without changing its shape. For any physical system which is governed by a set of nonlinear equations which admit a soliton solution, the nonlinear equations will, to some extent, be an approximation. During the formation of a Raman soliton, the soliton soliton is a poor approximation. Nonetheless, the forming pulse is often referred to as a soliton.

Due to the stability of the SRS soliton, Bowden and Englund[11,35,36] predicted that

quantum fluctuations during spontaneous emission in a Raman generator can lead to spontaneous soliton generation. These solitons appear as a macroscopic affect of quantum fluctuations. Experimental observations of spontaneous solitons are presented in Chapter 6.

The thesis is organized in the following manner. In Chapter 2 the equations needed to describe stimulated Raman scattering are derived in detail. The solution to these equations is then given for various approximations. Chapter 3 describes the use of localized modes for theoretically generating ensemble members of Stokes pulses from a Raman generator. Other methods of generating ensemble members are also used. Chapter 4 describes the experiment that we performed to measure statistics associated with quantum noise. A theoretical treatment of soliton generation in SRS is given in Chapter 5 and the soliton experiment is discussed in Chapter 6. Chapter 7 contains a summary of what we have accomplished.

CHAPTER 2

DERIVATION AND SOLUTION OF SRS EQUATIONS

To describe Stimulated Raman Scattering (SRS) before pump depletion, two coupled differential equations are needed. One equation describes how the Stokes pulse evolves from one location in the medium to the next due to an oscillating polarization in the medium. The other equation describes how the medium responds to the driving pump and Stokes fields. The Raman scattering process converts photons from the input pump pulse to photons of lower frequency in the Stokes pulse. If a significant number of photons are taken from the pump pulse, the shape of its temporal envelope will change. If this occurs a third equation is needed to describe how the pump pulse is depleted by the polarization in the medium and the Stokes field.

In this chapter the mathematics for treating the generation of a Stokes pulse from quantum noise and its subsequent amplification is developed. In the first section, the equation of motion for the polarization in the medium is presented. This derivation is outlined by Raymer and Mostowski[16] but the treatment given here fills in a lot of steps and gives a more complete explanation of the approximations used. In the second section the equation governing the growth of the Stokes field is derived from the system Hamiltonian. This derivation was done independently and I have not found a similar derivation in the papers which I have read. Normally Maxwell's equation for the field is used without being derived from the Hamiltonian. In the later sections, solutions to the SRS equations are presented for various approximations.

For the reader who is not interested in the details of how the equations are derived, the

operator equations for the Stokes field and polarization in the medium are given in Equations 2.27 and 2.55. The properties of the Langevin noise operator are important for understanding quantum noise so reading should continue in the third section.

A Raman generator can effectively be divided into three regions. In the first region, which is the quantum initiation region, the Stokes field grows from quantum noise to an amplitude which is large enough that the fields can be treated classically. The second region is the linear growth region where the Stokes growth can be modeled by two coupled linear equations and the pump can be assumed to be a prescribed input field. The linear region extends from the quantum initiation region to the location in the medium where the pump intensity has measurable depletion. The third region is the nonlinear growth region. In this region the dynamics of the pump field must be taken into account. This adds a third equation to the system and it becomes nonlinear. A general solution exists for the quantum initiation and linear regions. However, a general solution for the nonlinear region exists only in the steady state approximation[37]. Two coupled equations, one for the medium and one for the Stokes field, are needed when modeling the Stokes evolution in the initiation and linear regions. To theoretically model the system in the nonlinear region, the results obtained by evaluation of the exact solution at the end of the linear region are used as inputs for numerical propagation through the nonlinear region.

The general solution to the linear equations properly accounts for the quantum nature of the Stokes light and the medium but cannot account for pump depletion. The nonlinear set of equations, which must be integrated numerically, are not well suited for treating the quantum initiation but they are appropriate for the linear region as well as the nonlinear region. Both methods are valid in the linear region so there is no problem changing from the quantum solution to the nonlinear equations in the linear region. If the quantum mechanical operators are replaced by c-numbers (classical variables) and appropriate fluctuating noise is used for the initial Stokes field, the nonlinear equations

can be used for the entire calculation[11,38].

The equations of motion for the Stokes field and the Raman medium are derived using the Heisenberg equation of motion, taking the full quantum nature of the Stokes field account. The pump field will be treated as a prescribed input classical field which is valid before pump depletion because of the large number of photons in the pump pulse. The hermitian conjugate of an operator which is normally designated by a dagger will be designated by a superscript "+". For some operators, it is necessary to designate the positive or negative frequency components. This is done by including a superscript "(+)" or "(-)" in parenthesis. The Hamiltonian for the system in the Heisenberg picture is[39]

$$\hat{H}(t) = \sum_j \sum_{i=1}^{3} \hbar\omega_i \hat{\sigma}_{ii}^j(t) + \sum_{\lambda} \hbar\omega_\lambda \hat{a}_\lambda^+(t)\hat{a}_\lambda(t) - \sum_j \hat{\mu}^j(t) \cdot \hat{E}(z^j, t) \tag{2.1}$$

where the $\hat{\sigma}_{ij}^j(t)$ are atomic operators for the jth atom which at $t = 0$ are explicitly written as $\hat{\sigma}_{ij}(0) = |i\rangle\langle j|$. The annihilation operator, $\hat{a}_\lambda(t)$, is the operator for the radiation mode having angular frequency ω_λ and which is quantized in a volume of length L and area A. Periodic boundary conditions are assumed, and the label λ designates both the wavelength of the mode and its polarization. The sum over λ should be interpreted as a sum over modes having a frequency near the Stokes frequency. The dipole moment operator for the jth atom is $\hat{\mu}^j(t)$. The first term in the Hamiltonian gives the energy associated with the free atoms, and the second term gives the free Stokes field energy. The third term represents the dipole interaction between the atoms and the fields. The dipole operator for the jth atom is[39]

$$\hat{\mu}^j(t) = \vec{\mu}_{12}\hat{\sigma}_{12}^j(t) + \vec{\mu}_{23}\hat{\sigma}_{23}^j(t) + \vec{\mu}_{12}^*\hat{\sigma}_{21}^j(t) + \vec{\mu}_{23}^*\hat{\sigma}_{32}^j(t) \tag{2.2}$$

where $\vec{\mu}_{12}$ and $\vec{\mu}_{23}$ are the dipole matrix elements between levels 1 and 2 and levels 2 and 3 respectively. For example the dipole matrix element between levels 1 and 2 is

$$\vec{\mu}_{12} = e \langle 1|\vec{x}|2\rangle \quad . \tag{2.3}$$

The total field operator, $\hat{\mathrm{E}} = \vec{E}_p + \hat{E}_s$, is the sum of the pump and Stokes fields. The classical pump fields are given by

$$\vec{E}_p(z,t) = \mathrm{E}_p(z,t)\exp[i(\omega_p t - k_p z)]\,\vec{\varepsilon}_p + \mathrm{E}_p^*(z,t)\exp[-i(\omega_p t - k_p z)]\,\vec{\varepsilon}_p \quad . \tag{2.4}$$

The Stokes field is expressed in terms of the slowly varying envelope operators $\hat{\mathrm{E}}_s^{(+)}(z,t)$ and $\hat{\mathrm{E}}_s^{(-)}(z,t)$ using the definition[16]

$$\hat{E}_s(z,t) = \hat{\mathrm{E}}_s^{(-)}(z,t)\exp[i(\omega_s t - k_s z)]\,\vec{\varepsilon}_s + \hat{\mathrm{E}}_s^{(+)}(z,t)\exp[-i(\omega_s t - k_s z)]\,\vec{\varepsilon}_s \tag{2.5}$$

where the (+) and (-) denote the positive and negative frequency components of the field. Note the slight difference in the type used to represent the various field quantities.

$\hat{\mathrm{E}}(z,t)$ is the total field operator.

$\vec{E}_p(z,t)$ is the total pump field.

$\mathrm{E}_p(z,t)$ ($\mathrm{E}_p^*(z,t)$) is the positive (negative) part of the pump field.

$\hat{E}_s(z,t)$ is the total Stokes field operator.

$\hat{\mathrm{E}}_s^{(+)}(z,t)$ ($\hat{\mathrm{E}}_s^{(-)}(z,t)$)is the positive (negative) part of the slowly varying Stokes field

operator.

$\hat{E}_s^{(+)}(z,t)$ ($\hat{E}_s^{(-)}(z,t)$)is the positive (negative) part of the Heisenberg Stokes field operator.

At this point I will not write $\hat{E}_s^{(+)}(z,t)$ and $\hat{E}_s^{(-)}(z,t)$ in terms of creation and annihilation operators because they can in general be different operators than those which appear in the Hamiltonian. The operators that appear in the Hamiltonian are Heisenberg operators and thus contain all of the time dependence of the field. Therefore when the equation of motion for the field operators is calculated using Equation 2.1 the field must be expressed in terms of the cavity mode operators.

Derivation of the Medium Equation

The derivation in this section is similar to that given in reference 16. To obtain the equations of motion for the atomic operators, the equation

$$i\hbar\frac{d\hat{O}}{dt} = [\hat{O}, \hat{H}] \tag{2.6}$$

is used where $\hat{O}$ is an arbitrary operator without explicit time dependence. Using Equation 2.6 and noting that $\hat{\sigma}_{im}^j \times \hat{\sigma}_{mk}^j = \hat{\sigma}_{ik}^j$, the equations of motion for the three atomic superposition operators are calculated to give

$$\frac{d\hat{\sigma}_{31}^j(t)}{dt} = i\omega_{31}\hat{\sigma}_{31}^j(t) + \frac{i}{\hbar}[\vec{\mu}_{12}\hat{\sigma}_{32}^j(t) - \vec{\mu}_{23}\hat{\sigma}_{21}^j(t)] \cdot \hat{E}(z^j,t) \tag{2.7}$$

$$\frac{d\hat{\sigma}_{21}^{j}(t)}{dt} = i\omega_{21}\hat{\sigma}_{21}^{j}(t) + \frac{i}{\hbar}\left[\vec{\mu}_{12}(\hat{\sigma}_{22}^{j}(t) - \hat{\sigma}_{11}^{j}(t)) - \vec{\mu}_{23}^{*}\hat{\sigma}_{31}^{j}(t)\right] \cdot \hat{E}(z^{j}, t) \tag{2.8}$$

$$\frac{d\hat{\sigma}_{32}^{j}(t)}{dt} = -i\omega_{23}\hat{\sigma}_{32}^{j}(t) + \frac{i}{\hbar}\left[\vec{\mu}_{23}(\hat{\sigma}_{33}^{j}(t) - \hat{\sigma}_{22}^{j}(t)) + \vec{\mu}_{12}^{*}\hat{\sigma}_{31}^{j}(t)\right] \cdot \hat{E}(z^{j}, t) \tag{2.9}$$

where $\omega_{ij} = \omega_i - \omega_j$ and the commutator, $[a, \sigma_{ij}] = 0$ has been used. It will be shown in the later part of this section that the Stokes field operator will be driven by $\hat{\sigma}_{13}$. To this end, Equations 2.8 and 2.9 are formally integrated and the results substituted into Equation 2.7. It is interesting to note that equations of motion for the diagonal operators are not needed partially because the assumption that $\langle\hat{\sigma}_{11}\rangle = 1$ (which is valid even for complete pump depletion) will eventually be made and partially because of the effective elimination of level 2. The results of integrating Equations 2.8 and 2.9 are

$$\hat{\sigma}_{21}^{j}(t) = \hat{\sigma}_{21}^{j}(0)\exp(i\omega_{21}t) + \frac{i}{\hbar}\int_{0}^{t}\exp[i\omega_{21}(t-t')] \left\{\vec{\mu}_{12}[\hat{\sigma}_{22}^{j}(t') - \hat{\sigma}_{11}^{j}(t')] - \vec{\mu}_{23}^{*}\hat{\sigma}_{31}^{j}(t')\right\} \cdot \hat{E}(z^{j}, t')dt' \tag{2.10}$$

$$\hat{\sigma}_{32}^{j}(t) = \hat{\sigma}_{32}^{j}(0)\exp(-i\omega_{23}t) + \frac{i}{\hbar}\int_{0}^{t}\exp[-i\omega_{23}(t-t')] \left\{\vec{\mu}_{23}[\hat{\sigma}_{33}^{j}(t') - \hat{\sigma}_{22}^{j}(t')] + \vec{\mu}_{12}^{*}\hat{\sigma}_{31}^{j}(t')\right\} \cdot \hat{E}(z^{j}, t')dt' \tag{2.11}$$

The initial conditions are that the system starts in the ground state and the initial atomic operators are $\hat{\sigma}_{21}^{j}(0) = |2\rangle\langle 1|$ and $\hat{\sigma}_{32}^{j}(0) = |3\rangle\langle 2|$. When the integrals in Equations 2.10 and 2.11 are performed and the results are substituted into Equation 2.7, only the terms that oscillate near ω_{31} need to be kept. The terms in the integrals containing $\hat{\sigma}_{31}^{j}$ have parts which oscillate at the frequency needed to drive the pump-Stokes transition. These terms arise from combinations of $\mathbf{E}_p(z^j,t)$ and $\mathbf{E}_p^*(z^j,t')$ and also from combinations of $\hat{\mathbf{E}}_s^{(-)}(z^j,t)$ and $\mathbf{E}_s^{(+)}(z^j,t')$ plus terms with the opposite time ordering. However these terms only lead to a Stark shift and thus they can be discarded for this part of the calculation. To see that they will lead to a Stark shift, note that each of these terms will generate a contribution that is proportional to the operator $i\hat{\sigma}_{31}^{j}(t)$ and thus could be accounted for by simply modifying ω_{31}. The only remaining way to produce an oscillation at ω_{31} is with a combination of $\mathbf{E}_p(z,t) \times \hat{\mathbf{E}}_s^{(+)}(z,t')$ or $\mathbf{E}(z,t') \times \hat{\mathbf{E}}^{(+)}(z,t)$ corresponding to the two possible time orderings shown in Figure 1. Therefore, only these parts of the field will be kept when calculating $\hat{\sigma}_{21}$ and $\hat{\sigma}_{32}$. Rewriting Equation 2.10 and keeping only the terms which can drive the pump-Stokes transition, we obtain

$$\hat{\sigma}_{21}^{j}(t) = \frac{i}{\hbar}\int_0^t \exp[i\omega_{21}(t-t')] \quad [\hat{\sigma}_{22}^{j}(t') - \hat{\sigma}_{11}^{j}(t')] \quad \{\mathbf{E}_p(z^j,t')\exp[i(\omega_p t' - k_p z)] \quad \vec{\mu}_{12}\cdot\vec{\varepsilon}_p$$
$$+\hat{\mathbf{E}}_s^{(+)}(z^j,t')\exp[-i(\omega_s t' - k_s z)] \quad \vec{\mu}_{12}\cdot\vec{\varepsilon}_s\}\,dt' \quad . \qquad (2.12)$$

To carry out the integrals in Equation 2.12, the Slowly Varying Envelope Approximation (SVEA) is used. The SVEA assumes that the envelopes of the fields vary much slower than the individual oscillation of the field. This is a very good approximation because the envelopes typically vary over nanoseconds and the oscillation times are typically femtoseconds. The SVEA is not enough justification by itself for simply pulling the field envelopes and the atomic operators out of the integral. The meaning of the lower limit of

the integral must first be understood. The lower limit tells us something about the initial conditions of the system. In the real atom there is damping which would wash out any information about the initial conditions. However, the damping is not very important either because the amplitude of the oscillation of the atom at the driving frequency reaches semiequilibrium on a time scale of a few oscillations. This is because the fields are so far off resonance. The lower limit only determines the point about which $\hat{\sigma}_{21}^{j}$ oscillates. The time dependence of the slowly varying quantities in the integral and the damping can slightly change the point about which $\hat{\sigma}_{21}^{j}$ oscillates; however, only the oscillating part will drive $\hat{\sigma}_{31}^{j}$. Damping will be important in the equation of motion for the operator $\hat{\sigma}_{31}$ because its magnitude will be limited by damping whereas the magnitude of $\hat{\sigma}_{21}$ is limited by detuning. A mathematical justification of the SVEA is given in Appendix A. Making the SVEA and evaluating the integral in Equation 2.12 at the upper limit results in

$$\hat{\sigma}_{21}^{j}(t) = -\frac{1}{\hbar}(\hat{\sigma}_{22}^{j}(t) - \hat{\sigma}_{11}^{j}(t))\left\{\frac{\exp[i(\omega_p t - k_p z)]}{(\omega_{21} - \omega_p)} \mathrm{E}_p \quad \vec{\mu}_{12} \cdot \vec{\varepsilon}_p \right.$$
$$\left. + \frac{\exp[-i(\omega_s t - k_s z)]}{(\omega_{21} + \omega_s)} \hat{\mathrm{E}}_s^{(+)} \quad \vec{\mu}_{12} \cdot \vec{\varepsilon}_s \right\} . \qquad (2.13)$$

And, similarly for $\hat{\sigma}_{32}^{j}(t)$, Equation 2.11 becomes

$$\hat{\sigma}_{32}^{j}(t) = \frac{1}{\hbar}(\hat{\sigma}_{33}(t)^{j} - \hat{\sigma}_{22}(t)^{j})\left\{\frac{\exp[i(\omega_p t - k_p z)]}{(\omega_{23} + \omega_p)} \mathrm{E}_p(z^{j}, t) \quad \vec{\mu}_{23} \cdot \varepsilon_p \right.$$
$$\left. + \frac{\exp[-i(\omega_s t - k_s z)]}{(\omega_{23} - \omega_s)} \hat{\mathrm{E}}_s^{(+)}(z^{j}, t) \quad \vec{\mu}_{23} \cdot \vec{\varepsilon}_s \right\} . \qquad (2.14)$$